Chemosphere 370 (2025) 143964

Contents lists available at ScienceDirect

Chemosphere

journal homepage: www.elsevier.com/locate/chemosphere

Long-range atmospheric transport of organochlorine pesticides from China to South Korea: Evidence from Deokjeok Island

Ho-Young Lee [a], Sung-Deuk Choi [a,b,*], Min-Kyu Park [a,1], Yoon-Se Lee [b], Chul-Su Kim [b], Cheol-Hee Kim [c], Lim-Seok Chang [d]

[a] Department of Civil, Urban, Earth, and Environmental Engineering, Ulsan National Institute of Science and Technology (UNIST), Ulsan, 44919, Republic of Korea
[b] UNIST Environmental Analysis Center (UEAC), Ulsan National Institute of Science and Technology (UNIST), Ulsan, 44919, Republic of Korea
[c] Department of Atmospheric Sciences, Pusan National University, Busan, 46241, Republic of Korea
[d] Climate and Air Quality Research Department, National Institute of Environmental Research, Incheon, 22689, Republic of Korea

HIGHLIGHTS

- OCP levels and their sources were assessed at a background site in South Korea.
- Gaseous OCPs were significantly influenced by past use.
- Particulate OCPs likely originated from recent emissions and LRAT.
- Consistent detection and modeling results provide strong evidence of LRAT for OCPs.
- Past use and LRAT play key roles in the dynamic environmental behavior of OCPs.

GRAPHICAL ABSTRACT

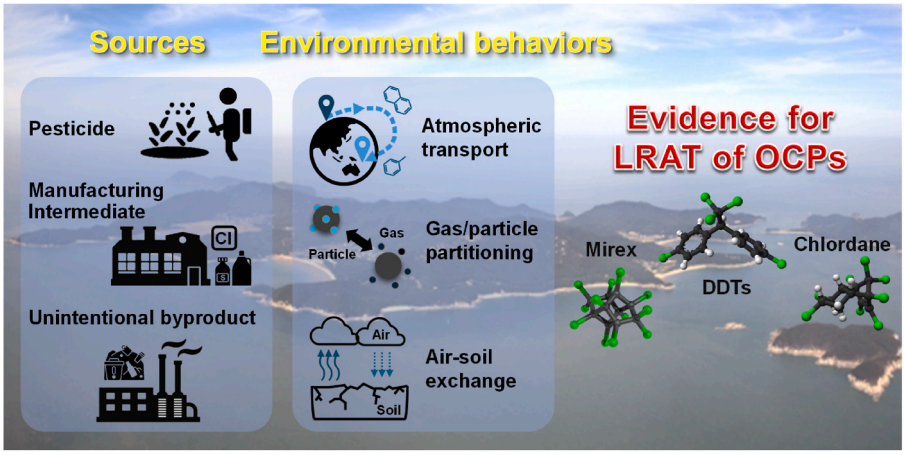

ARTICLE INFO

Keywords:
LRAT
OCPs
POPs
Deokjeok Island
Fugacity fraction

ABSTRACT

The influence of transboundary air pollutants originating from the Asian continent on South Korea has been a major concern. Although organochlorine pesticides (OCPs) have been banned for several decades, they continue to be detected in the Korean environment. However, studies on the long-range atmospheric transport (LRAT) of OCPs in South Korea, particularly in background areas, remain limited. This study investigated the atmospheric levels, sources, and behavior of OCPs at Deokjeok Island, a background site near the west coast of the Korean Peninsula. Total concentrations of 24 OCPs ranged from 53.6 to 325 pg/m^3, which are lower than those reported by the national POPs monitoring network of South Korea and similar to levels found in other background regions

* Corresponding author. Department of Civil, Urban, Earth, and Environmental Engineering, Ulsan National Institute of Science and Technology (UNIST), Ulsan, 44919, Republic of Korea.
E-mail addresses: hylee@unist.ac.kr (H.-Y. Lee), sdchoi@unist.ac.kr (S.-D. Choi), mkpark86@unist.ac.kr (M.-K. Park), 30296@unist.ac.kr (Y.-S. Lee), kimcs@unist.ac.kr (C.-S. Kim), chkim2@pusan.ac.kr (C.-H. Kim), lschang@korea.kr (L.-S. Chang).
[1] Present address: Department of Environmental Engineering, Jeju National University, Jeju, 63243, Republic of Korea.

https://doi.org/10.1016/j.chemosphere.2024.143964
Received 9 September 2024; Received in revised form 2 December 2024; Accepted 14 December 2024
Available online 20 December 2024

in Northeast Asia. HCB (62.7 pg/m^3, 45%) and PeCB (46.6 pg/m^3, 33%) were the most dominant OCPs in the gaseous phase, whereas DDTs were predominant (1.65 pg/m^3, 44%) in the particulate phase. Gaseous OCPs were strongly influenced by past use and re-emissions, while ongoing emissions and LRAT were the major sources of particulate OCPs. The consistent detection of mirex provides strong evidence of LRAT. In addition, correlation analysis and the Clausius-Clapeyron equation indicated that DDTs were significantly influenced by LRAT. Concentration-weighted trajectory maps identified East, North, and Northeast China as the major source regions for gaseous OCPs, driven by re-emissions, while the primary source areas for particulate OCPs were Beijing, Hebei, Tianjin, and Shandong. Air/soil fugacity fractions showed equilibrium or net deposition for most OCPs (except PeCB), indicating the dynamic environmental behavior of OCPs influenced by past use and LRAT. This study provides evidence of LRAT of OCPs to South Korea, demonstrating the significant impact of transboundary pollution. These results highlight the importance of ongoing monitoring of both historically and currently used pesticides at receptor sites in Northeast Asia.

1. Introduction

Organochlorine pesticides (OCPs), a group of persistent organic pollutants (POPs), were widely used in agricultural activities during the 1950s–1960s (Li and Macdonald, 2005). They were subsequently banned in the 1980s due to their toxicity, except in specific cases related to public health and malaria control in some countries (Angulo Lucena et al., 2007). The persistence, semi-volatility, and potential for long-range atmospheric transport (LRAT) of OCPs have continuously raised concerns about their environmental impact (Kallenborn et al., 2007; Gong et al., 2010). Legacy OCPs, such as hexachlorocyclohexanes (HCHs), dichlorodiphenyltrichloroethanes (DDTs), chlordanes (CHLORs), and mirex, are still detected in the atmosphere, even in regions where their manufacture and use have been prohibited (Wang et al., 2018b; Iakovides et al., 2021). These banned OCPs continue to be emitted into the atmosphere from both primary and secondary sources in terrestrial and marine environments (Wang et al., 2012; Li et al., 2020). Atmospheric transport plays a significant role in the distribution of released OCPs, leading to their presence even in remote areas (Wang et al., 2012, 2018b; Ding et al., 2022). Therefore, atmospheric monitoring of OCPs and understanding the impact of LRAT are crucial.

The residue levels of OCPs in the atmosphere can be attributed to two key factors: re-emission from environmental reservoirs and LRAT. Generally, OCP concentrations increase during warm seasons due to enhanced re-emission from environmental matrices (Qu et al., 2015; Khuman et al., 2023). Subsequently, OCPs can migrate to other regions under warm conditions through atmospheric transport and deposition (Wania and Mackay, 1993). OCPs exist in both gaseous and particulate phases, and their LRAT should be considered separately due to the distinct environmental behaviors of each phase (Yu et al., 2019). Furthermore, understanding the partitioning between these two phases is crucial for identifying sources, assessing LRAT effects, and determining the environmental fate of OCPs. Equilibrium state models, such as the Junge-Pankow (J-P) model and the octanol-air partition coefficient (K_{OA}) absorption model, have been widely used to study the gas/particle (G/P) partitioning behavior of OCPs (Harner and Bidleman, 1998; Wang et al., 2023). In addition, air/soil exchange processes (i.e., atmospheric deposition and evaporation from surface matrices) play a key role in determining their environmental fate (Chakraborty et al., 2015; Zhan et al., 2017). These environmental behaviors are influenced by both environmental parameters and the physicochemical properties of the chemicals (Odabasi and Cetin, 2012; Qu et al., 2015). Therefore, LRAT effects, G/P partitioning behavior, and air/soil exchange should be considered to gain a thorough understanding of atmospheric transport pathways and the environmental fate of OCPs.

In Northeast Asia, OCPs have been heavily used historically in South and East China (Tian et al., 2009), and these regions are considered sources of OCPs for North China, South Korea, and Japan (Takazawa et al., 2016; Wang et al., 2023). Moreover, high levels of particulate matter (PM) facilitate the transport of particulate-bound OCPs into South Korea (Jin et al., 2013). Consequently, South Korea is particularly susceptible to receiving OCPs from the northeastern Asian continent. In South Korea, approximately 3,600 tonnes of OCPs were used for agricultural purposes until their ban in the 1980s (Kang et al., 2008). To regulate and monitor various POPs, the Korean Ministry of Environment (KMOE) established a nationwide POPs monitoring program in 2008 under the POPs Control Act. The status of POPs in multimedia environments (air, soil, and water) is reported annually, and several studies on air monitoring have been conducted. For example, residual levels of OCPs at 37 nationwide stations and the impact of LRAT were investigated (Park et al., 2011). Recently, long-term monitoring results of atmospheric OCPs from 2008 to 2017 were interpreted, and decreasing trends associated with regulatory actions were highlighted (Khuman et al., 2023). Additionally, the occurrence, seasonal variability, and sources of OCPs at background sites (Baengnyeong and Jeju Island) and urban sites (Seoul and Seosan) were investigated (Lee et al., 2022), indicating that OCPs still exhibit relatively high levels, despite being banned in South Korea (Park et al., 2011).

The goal of this study is to identify the sources of OCPs in the atmosphere and determine their atmospheric transport pathways and environmental fate. Gaseous and particulate samples were collected on Deokjeok Island in South Korea, and the pollution levels and profiles of 24 OCPs were analyzed. Source identification of OCPs was conducted based on meteorological parameter analysis and backward air trajectory modeling. Furthermore, to understand their environmental behaviors, G/P partitioning and air/soil fugacity fractions were investigated.

2. Materials and methods

2.1. Study area and sample collection

Deokjeok Island is located on the western coast of the Korean Peninsula, approximately 50 km from Seoul Metropolitan City. The sampling sites were located on the south beach (37.2151°N, 126.1408°E), away from potential pollution sources such as ports to the north and farmland to the east (Fig. 1). Meteorological parameters, including air temperature, wind direction, wind speed, and precipitation, were measured at an automatic weather station operated by the Korea Meteorological Administration, located east of the sampling site. In addition, PM_{10} concentrations were measured at an air quality monitoring station operated by the National Institute of Environmental Research.

High-volume air samplers (HiVol, HV-700F, Sibata, Japan) were used to collect both gaseous and particulate (total suspended particulate: TSP) samples on polyurethane foam (PUF) plugs and glass fiber filters (GFFs), respectively. Duplicate HiVol samples were collected for 24 h starting at 11:00 a.m. for 10 days, from May 21 to May 26 and from July 24 to July 29, 2013. The total air sampling volume was 1007.9 m^3 with a flow rate of 700 L/min for each sample. Surface soil samples (<5 cm) were collected at four sites on both May 26 and July 29, with each sample composed of five sub-samples. Triplicate passive air samplers equipped with polyurethane foam disks (PUF-PAS) were deployed for 64 days (May 26–July 29) at a nearby soil sampling site. The air and soil samples were transported to the laboratory and stored in polyethylene

zippered bags at −4 °C until analysis. Prior to sampling, PUF plugs and disks were cleaned using a sonicator for 30 min with acetone and hexane to remove water and organic contaminants, respectively. GFFs were baked at 400 °C for 16 h to remove organic substances. The soil samples were dried at room temperature, homogenized, and sieved using a 2-mm steel sieve before analysis.

2.2. Chemical analysis

The PUF plug, GFF, PUF disk, and soil samples were separately Soxhlet extracted, and the extracts were purified using neutral silica gel columns. Twenty-four individual target OCPs, including hexachlorobenzene (HCB), pentachlorobenzene (PeCB), 4 HCHs, 6 DDTs, 5 CHLORs, 3 heptachlors (HEPs), 3 DRINs (aldrin, dieldrin, and endrin), and mirex, were analyzed using a gas chromatograph/high-resolution mass spectrometer (GC/HRMS) (AutoSpec Premier, Waters, USA). A detailed description of the analytical procedure is provided in Text S1 in the Supplementary Information.

For quality assurance and quality control (QA/QC), the recoveries of surrogate standards were calculated for each PUF plug, GFF, PUF disk, and soil sample. Instrumental detection limits (IDLs) and method detection limits (MDLs) were calculated by multiplying the Student's *t* value at 99% confidence (3.14) by the standard deviation (SD) of seven replicates for the lowest calibration standard (0.4 pg/μL) and the spiked PUF plug and GFF blank samples (30 pg spiked, assuming 0.1 pg/m^3), respectively. For soil, MDLs were determined based on signal-to-noise (S/N) ratios of 3:1 in the soil samples. The IDLs and MDLs are listed in Table S1 in the Supplementary Information. Field blanks were collected to assess contamination introduced during sample collection and pretreatment in the laboratory. These blank samples were pre-treated and analyzed for the target OCPs following the same procedure as the real samples. The mean concentration of each compound (HCB, PeCB, α-HCH, and δ-HCH) in the field blanks was subtracted from that of the real samples. Concentrations below the MDLs were treated as non-detected (ND). The mean recoveries of surrogate standards from the PUF plug, GFF, PUF disk, and soil samples were 75%, 92%, 68%, and 70%, respectively. Compound- and matrix-specific mean recoveries are provided in Table S1.

2.3. Source identification

2.3.1. Statistical analysis

The normality of the OCP data was assessed using SigmaPlot 14.0 (Systat Software Inc., USA). As the data were not normally distributed, non-parametric tests (Mann-Whitney rank sum test and Spearman correlation analysis) were conducted using SigmaPlot 14.0 and SPSS Statistics 25 (IBM, USA), respectively. The Mann-Kendall test was conducted to identify trends in OCPs, and Sen's slope was used to estimate the magnitude of increase or decrease in the trend, using the 'trend' package in R software (version 4.0.2, R core Team, Austria).

2.3.2. Influence of meteorological parameters

The relationships between OCPs and meteorological parameters were investigated using Spearman correlation analysis. The Clausius-Clapeyron (*CC*) equation was used to investigate the temperature dependence of individual OCPs using Eq. (1), as described elsewhere (Sofuoglu et al., 2004; Stojić and Stanišić Stojić, 2017).

$$\ln P = \left(\frac{-\Delta H_v}{R}\right) \bullet \left(\frac{1}{T}\right) + \text{constant} \quad (1)$$

where P is the partial pressure, R is the gas constant (8.314 J/mol·K), T is the temperature, and ΔH_v is the enthalpy of vaporization (kJ/mol). ln P is regressed against the inverse of T, and the resulting linear slope describes the temperature dependence of individual OCPs. While the slope of the *CC* equation can be used to calculate ΔH_v, it represents the enthalpy of surface-air exchange (ΔH_{sa}) under the given environmental conditions. This value reflects the energy required for a phase transition from the surface to the atmosphere (Wania et al., 1998).

2.3.3. Backward air trajectory analysis

Backward air trajectories at the sampling site were calculated using the Hybrid Single-Particle Lagrangian Integrated Trajectory (HYSPLIT 5) model, developed by the National Oceanic and Atmospheric Administration (https://www.arl.noaa.gov/hysplit/). Three-day (72 h) backward air trajectories were calculated every hour for the HiVol sampling days, starting at a height of 500 m above ground level. Reanalysis data from the National Centers for Environmental Prediction and the National Center for Atmospheric Research (NCEP/NCAR) were used as input meteorological data with a resolution of 2.5° × 2.5°. A total of 240 trajectories were obtained for the HiVol sampling period. Daily backward air trajectories are illustrated in Fig. S1 in the Supplementary Information.

The concentration-weighted trajectory (CWT), a hybrid-receptor model, was used to identify potential regional emission sources and LRAT of OCPs. The CWT assigns a weighted concentration of the target OCP by associating trajectories in each grid cell based on Eq. (2).

$$CWT_{ij} = \frac{\sum_{l=1}^{M} C_j \, \tau_{ijl}}{\sum_{l=1}^{M} \tau_{ijl}} \quad (2)$$

where M is the total number of backward trajectories, τ_{ijl} represents the number of endpoints in cell (i, j) for trajectory l, and C_j is the OCP concentration. TrajStat software (1.4.4R5, Chinese Academy of Meteorological Sciences, China) was used to calculate CWT values with a grid

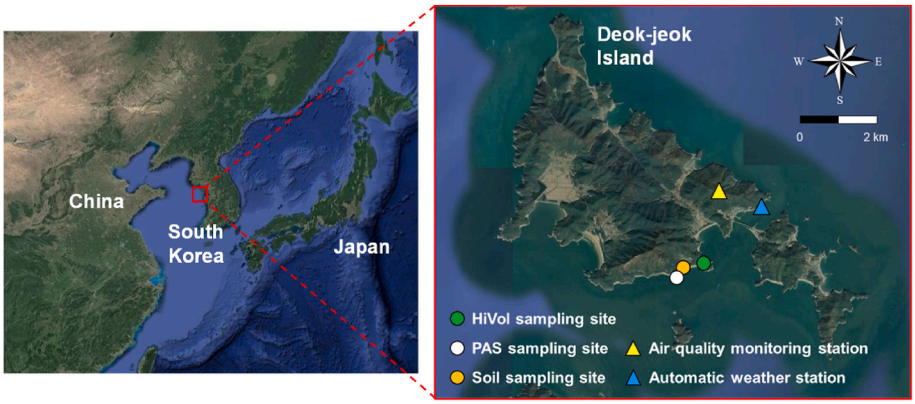

Fig. 1. Locations of sampling sites on Deokjeok Island, South Korea. The air quality monitoring station and the automatic weather station are also marked.

cell size of 0.5° × 0.5°. A weighted function $W(n_{ij})$, as described in Eq. (3), was used to reduce the trailing effect, which indicates the high uncertainty of the source area due to a small number of trajectories passing through the grid cell (Stojić and Stanišić Stojić, 2017). Areas with higher CWT values are expected to be potential source regions of OCPs.

$$W(n_{ij}) = \begin{cases} 1, 2av \le n \\ 0.75, av \le n < 2av \\ 0.5, 0.5av \le n < av \\ 0.25, n < 0.5av \end{cases} \quad (3)$$

where n_{ij} is the number of trajectory endpoints in grid cell (i, j), and av is the average number of trajectory endpoints per cell. In addition, cluster analysis was performed using the Euclidean distance method. The number of clusters was determined to be two based on the change in total spatial variance (TSV), which is the sum of the cluster spatial variance values (Draxler et al., 2020).

2.4. Gas/particle partitioning model

The G/P partitioning model for OCPs was used to study their partitioning behavior and equilibrium. First, the partitioning behavior of OCPs was investigated by fitting the measured data to the Junge-Pankow G/P partitioning model. This model, which is based on the fraction in the particulate phase (φ), is more suitable for fitting OCP data than using linear regressions with the gas/particle partition coefficient. Second, two equilibrium-state models, the K_{OA} absorption model (Harner and Bidleman, 1998) and the steady-state model (Li et al., 2015), were used to predict the equilibrium partitioning coefficient (K_{PE}) and the steady-state partitioning coefficient (K_{PS}). The measured G/P partitioning coefficient (K_P) was calculated using the concentrations of the particulate and gaseous phases, normalized by the TSP concentration, and then compared with the predicted values to evaluate the partitioning behavior of OCPs. The steady-state model was found to be more suitable for predicting K_P values for OCPs, as it accounts for the influence of wet and dry deposition on partitioning Qiao et al. (2019); OriginPro 2020 (OriginLab, USA) was used for G/P partitioning modeling. Detailed descriptions of the calculations and model parameters are provided in Text S2 and Table S2, respectively.

2.5. Fugacity fractions

To assess the net transfer of OCPs between air and soil, fugacity fractions were calculated using air and soil concentration data. Air concentrations of OCPs were calculated based on the accumulated amounts in PUF-PAS. A detailed calculation method for atmospheric OCP concentrations using PUF-PAS is provided in Text S3. Air and soil data for 12 OCPs, which exhibited high detection frequencies in both PUF disk and soil samples, were selected to calculate fugacity fractions. The air/soil concentration ratios (A/S) for OCPs were calculated using soil density based on the following Eqs. (4) and (5):

$$A \Big/ S = \frac{C_A}{\rho_S \bullet C_S} \quad (4)$$

$$\rho_S = f_{OC} \bullet \rho_{OC} + (1 - f_{OC}) \bullet \rho_{SM} \quad (5)$$

where C_A is the measured air concentration in ng/m^3, C_S is the measured soil concentration in ng/kg, and ρ_S is the density of soil solids in kg/m^3. The density of soil solids was calculated using the organic carbon fraction (f_{OC}) of soil samples, along with the density of soil organic carbon (ρ_{OC}: 1,000 kg/m^3) and the density of mineral matter (ρ_{SM}: 2,650 kg/m^3) (Daly et al., 2007). The f_{OC} in the soil samples was determined using the loss-on-ignition (LOI) method, which quantifies the weight change of the sample before and after the combustion of organic matter at high temperatures. It was assumed that the LOI value was equal to f_{OM}, and f_{OC} was calculated by multiplying f_{OM} by an empirical constant (the van Bemmelen value of 0.58) (Choi, 2014). To express the air-soil equilibrium, the fugacity fraction (F) between air and soil was calculated using Eq. (6):

$$F = \frac{f_S}{f_S + f_A} = \frac{1}{1 + E \bullet f_{OC} \bullet \rho_S \bullet K_{OA} \bullet A/S} \quad (6)$$

where f_S and f_A represent the fugacity in soil and air, respectively, and E is an empirical constant (0.00075 m^3/kg) (Hippelein and McLachlan, 1998). The partitioning of OCPs to soil is primarily driven by the absorption process into the organic carbon fraction, indicating that K_{OA} is an important property for partitioning between air and soil (Harner and Bidleman, 1998). The K_{OA} values were adjusted for the ambient air temperature of each sampling day using the temperature-dependent equations from Shoeib and Harner (2009).

3. Results and discussion

3.1. Levels of OCPs

3.1.1. Variations in levels and patterns of OCPs

Daily concentrations of Σ_{24} OCPs and the fractions of OCP groups in the total (gas + particle) phases are presented in Fig. 2. Compound-specific concentrations are provided in Table S3. The concentrations of Σ_{24} OCPs in both phases ranged from 53.6 to 325 pg/m^3 with a mean of 144 pg/m^3. The concentration of Σ_{24} OCPs was higher in May (mean: 173 ± 123 pg/m^3, median: 153 pg/m^3) than in July (mean: 115 ± 25.2 pg/m^3, median: 120 pg/m^3); however, the difference was not statistically significant (rank sum test, $p > 0.05$). The notable variation in daily concentrations of Σ_{24} OCPs can be attributed to the fluctuations in two dominant OCPs, HCB and PeCB. In particular, their levels were much higher on May 22–23 (HCB: 102 pg/m^3 and PeCB: 162 pg/m^3) compared to other days (HCB: 53.7 pg/m^3 and PeCB: 18.1 pg/m^3). A previous study reported that atmospheric levels of HCB and PeCB in South Korea were higher in the summer due to increased volatilization at higher temperatures (Lee et al., 2022). In contrast, HCB levels in East China were highest in winter, strongly associated with combustion sources (Mao et al., 2020). The elevated levels of HCB and PeCB in May, when ambient temperatures were lower and volatilization was reduced, can be attributed to the influence of inflow from China. The influence of LRAT on OCPs will be discussed in Section 3.3.2.

HCB accounted for the highest fraction (63.3 pg/m^3, 44%) of the concentrations of Σ_{24} OCPs, followed by PeCB (46.9 pg/m^3, 33%), HCHs (13.8 pg/m^3, 9.6%), DDTs (13.0 pg/m^3, 9.0%), CHLORs (3.65 pg/m^3, 2.5%), HEPs (1.30 pg/m^3, 0.9%), mirex (1.05 pg/m^3, 0.7%), and DRINs (0.99 pg/m^3, 0.7%) (Fig. 2). HCB and PeCB were also the most dominant compounds monitored at background sites in China (Zhan et al., 2017) and Switzerland (Kirchner et al., 2016), attributed to ongoing sources from surrounding areas. In South Korea, HCB and PeCB have not been used as pesticides but only as intermediates in manufacturing processes (Park et al., 2011). Therefore, the high concentrations of HCB and PeCB observed in this study can be explained by atmospheric transport and secondary emissions from surface environments. Among the other OCP groups, HCHs contributed the highest proportions (13.8 pg/m^3, 9.6%) to total Σ_{24} OCPs, with α-HCH (9.66 pg/m^3, 71%) as the most dominant isomer in the HCH group (Fig. S2). DDTs had the fourth-highest proportion within the total Σ_{24} OCPs, with o,p'-DDE (4.67 pg/m3, 38%) being the most prevalent isomer.

The levels and patterns of OCPs observed in this study are consistent with those reported in previous studies in South Korea (Lee et al., 2022; Khuman et al., 2023). The current levels of these compounds were mainly influenced by historical usage, such as the application of technical HCH and DDT (Khuman et al., 2023). The elevated levels of Σ_{24} OCPs on May 22 (270 pg/m^3) and May 23 (323 pg/m^3) suggest a potential influence of external inflow. According to daily wind rose plots,

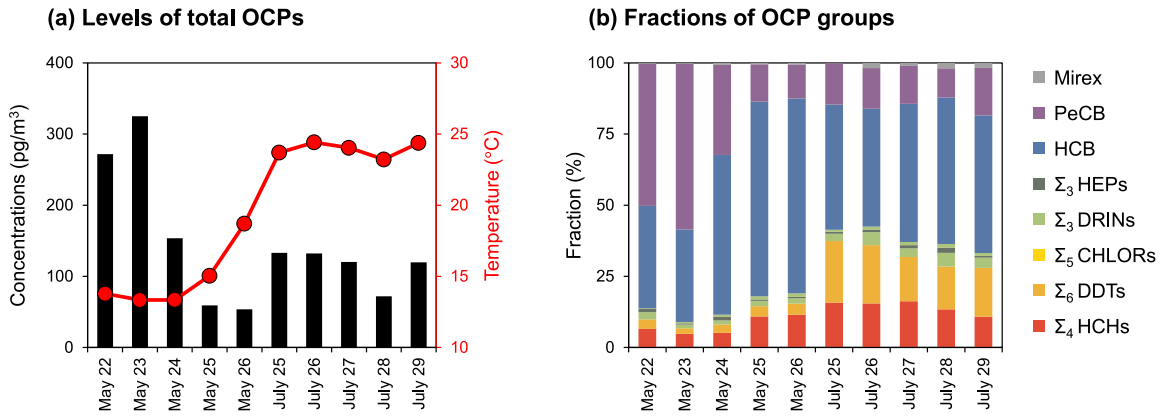

Fig. 2. Daily (a) levels of total (Σ_{24}) OCPs and (b) fractions of individual OCP groups, along with daily ambient air temperatures.

southerly and westerly winds prevailed on May 22 and May 23, respectively (Fig. S1). Backward trajectory analysis revealed similar transport pathways for both days, suggesting the influence of LRAT. Further discussions on the source identification of OCPs based on meteorological conditions are presented in Section 3.3.

3.1.2. Comparison with previous monitoring studies

The levels of OCPs in this study were compared with those from the national POPs monitoring network of South Korea (Table 1). The nationwide mean concentration of Σ_{18} OCPs in 2008 (161 pg/m^3) (Park et al., 2011) was higher than the mean concentration of Σ_{18} OCPs in this study (83.3 pg/m^3). The nationwide mean concentration of Σ_{23} OCPs in 2013 (311 pg/m^3), which included 4 HCHs and mirex as additional target compounds (KMOE, 2015), was 3.4 times higher than the concentration of Σ_{23} OCPs (excluding PeCB) observed in this study (97.1 pg/m^3). In particular, the nationwide concentrations of HCBs (237 pg/m^3), HCHs (33.2 pg/m^3), and CHLORs (33.3 pg/m^3) were 3.7, 2.4, and 9.1 times higher, respectively, than those in this study. The nationwide concentration of Σ_{23} OCPs (excluding PeCB) significantly decreased (Mann-Kendall test, $p < 0.05$) from 311 pg/m^3 in 2013 to 187 pg/m^3 in 2019 (KMOE, 2018). Meanwhile, the annual mean concentrations of PeCB remained relatively stable (mean: 113 pg/m^3, Mann-Kendall test, $\tau = -0.06$) over the years, with the highest concentrations in 2019 (131 pg/m^3) and the lowest in 2016 (91.2 pg/m^3) (KMOE, 2017). The stable PeCB levels in South Korea may be influenced by consistent sources, including unintentional byproduct releases from industrial processes and the use of chlorinated compounds (Bailey et al., 2009). A previous study also reported a decreasing trend in nationwide mean OCP concentrations from 2008 to 2017, attributed to regulatory actions (Khuman et al., 2023). However, the concentrations of DDTs (13.0 ± 10.1 pg/m^3) and mirex (1.05 ± 0.74 pg/m^3) in this study were higher than those in the national POPs monitoring network (KMOE, 2015), providing strong evidence of re-volatilization from surface environments and LRAT. Elevated levels of DDTs have also been observed in various urban areas across China (mean: 28.5 pg/m^3) (Wang et al., 2023), and mirex concentrations at Mount Tai, China (mean: 10.1 pg/m^3) (Liu et al., 2019) were notably higher than those observed in background regions of South Korea. The relatively high concentrations of DDTs and mirex in China suggest that these compounds are more susceptible to LRAT. The mean concentrations of OCPs in this study were comparable to those found in background areas in South Korea, such as Gosan (Jeju), Goesan, and Taean in 2008 (Σ_{17} OCPs: 246 pg/m^3) (Jin et al., 2013) and Jeju and Baengnyeong islands in 2020 (Σ_{22} OCPs: 190 pg/m^3) (Lee et al., 2022). These findings suggest that the levels and sources of OCPs have remained relatively constant, attributed to similar atmospheric transport pathways and continuous volatilization in background regions.

A continental-scale monitoring study conducted in China, South Korea, and Japan in 2004 (Jaward et al., 2005), reported that HCB levels in China (10.4–462 pg/m^3) were higher than those in South Korea (26.0–136 pg/m^3) and Japan (14.1–94.7 pg/m^3). DDT concentrations in China, with a mean of 23.6 pg/m^3 in 2013 and 205 pg/m^3 in 2016, were dramatically higher than those in South Korea (annual nationwide means: 4.24 pg/m^3 in 2013 and 2.56 pg/m^3 in 2016) (Table 1), primarily due to significant DDT production in China for malaria control until 2007 (Qiu et al., 2005). Despite the ban on most OCPs in China, their legacy use has resulted in consistently high concentrations, as accumulated OCPs in soil and water continue to be emitted and transported to surrounding areas (Ding et al., 2022). In particular, urban sites in China exhibited much higher OCP concentrations, with the mean concentration of Σ_{17} OCPs reaching 850 pg/m^3 in 2006 (Yang et al., 2008), with elevated concentrations of CHLORs and DDTs. Σ_{24} OCP concentrations in northern coastal cities of China were recorded at 1, 519 pg/m^3 in 2016 (Yu et al., 2019). Previous studies also monitored various OCPs at background sites in Qinghai, China (Σ_{11} OCPs: 321 pg/m^3) (Cheng et al., 2007) and at a China Atmosphere Watch Network (CAWNET) site in Hubei (Σ_{15} OCPs: 191 ± 107 pg/m^3) (Zhan et al., 2017). OCP levels in these background areas, which have low influence from local re-emissions (Zhan et al., 2017), were considerably lower than those in urban areas (405 pg/m^3) (Wang et al., 2023). In Japan, a nationwide monitoring study reported steady levels of HCB (104 pg/m^3) and PeCB (60 pg/m^3) between 2003 and 2018, with slight increases (Dien et al., 2021). Monitoring of HCHs and CHLORs on Okinawa Island from 2009 to 2014 did not show clear annual trends, displaying only seasonal variations (Takazawa et al., 2016). However, DDT levels on Okinawa Island significantly decreased during the same period, with diagnostic ratios indicating fresh inputs from Northeast Asia. In Mongolia, HCB, HCH, and DDT concentrations were reported at 15.8 pg/m^3, 38.3 pg/m^3, and 252 pg/m^3, respectively, at urban sites in 2009 (Mamontova et al., 2011). The Northern Hovsgol region, a background area in Mongolia, showed a decreasing trend in DDTs (from 70 pg/m^3 in 2008 to 13 pg/m^3 in 2015) and HCHs (from 35 pg/m^3 in 2008 to 15 pg/m^3 in 2015) (Mamontova et al., 2019). Overall, OCP levels in receptor areas affected by LRAT in Northeast Asia, such as background sites in South Korea, Japan, and Mongolia, have been steadily decreasing.

3.2. Profiles and diagnostic ratios of OCPs

The mean level of gaseous OCPs (140 pg/m^3) was much higher than that of particulate OCPs (3.71 pg/m^3). The composition of gaseous OCPs was similar to that of total (gas + particle) OCPs, while the composition of particulate OCPs differed (Fig. 3a). Gaseous OCPs contributed over 80% of the total OCPs, except for *p,p'*-DDT (47%) and dieldrin (50%)

Table 1
Comparison of atmospheric OCP concentrations (pg/m^3) measured in South Korea and other countries in Northeast Asia.

Country	Period	Target OCPs	Σ OCPs	Σ_4 HCHs	Σ_6 DDTs	Σ_5 CHLORs	Σ_3 HEPs	Σ_3 DRINs	HCB	PeCB	Mirex	Reference
Deokjeok Island, Korea	2013	24	144 ± 88.9 (53.6–325)	13.8 ± 5.90 (6.19–21.0)	13.0 ± 10.1 (2.10–28.8)	3.65 ± 1.94 (1.00–7.01)	1.30 ± 0.92 (0.25–3.43)	0.99 ± 0.37 (0.31–1.41)	63.3 ± 24.9 (36.7–106)	46.9 ± 63.3 (6.38–189)	1.05 ± 0.74 (0.13–2.35)	This study
Nationwide 37 sites, Korea	2008	18	161	–	5.24 (ND–47.6)	5.76 (ND–39.0)	1.28 (ND–9.19)	0.66 (ND–9.30)	148 (41.2–344)	–	–	Park et al. (2011)
Nationwide 38 sites, Korea	2013	23	311	33.3 ± 36.0 (8.23–224)	4.24 ± 3.78 (0.35–17.0)	33.3 ± 15.5 (5.42–73.3)	1.95 ± 0.86 (0.48–4.35)	1.45 ± 0.88 (ND–3.81)	237 ± 101 (86.6–598)	–	0.11 ± 0.27 (ND–1.06)	KMOE (2015)
	2016	24	308	24.1 ± 14.6 (8.48–78.8)	2.56 ± 2.50 (ND–11.2)	1.82 ± 1.20 (ND–4.68)	0.41 ± 0.35 (ND–1.70)	0.63 ± 0.79 (ND–3.94)	187 ± 85.0 (106–587)	91.2 ± 42.4 (42.9–261)	0.25 ± 0.61 (ND–2.35)	KMOE (2017)
	2019	24	313	16.1 ± 11.2 (5.55–63.1)	1.45 ± 2.61 (ND–12.9)	0.98 ± 4.79 (ND–15.3)	0.10 ± 0.13 (ND–1.91)	0.11 ± 0.74 (ND–3.14)	164 ± 76.3 (6.52–351)	131 ± 106 (40.9–480)	ND	KMOE (2018)
Gosan, Goesan, and Taen, Korea	2008–2009	17	246 ± 179 (37.7–700)	141 ± 153 (10.8–542)	6.22 ± 9.92 (ND–56.5)	2.38 ± 2.72 (ND–10.5)	0.78 ± 0.67 (ND–2.59)	1.08 ± 1.13 (ND–4.36)	94.1 ± 56.8 (15.0–256)	–	0.09 ± 0.14 (ND–0.78)	Jin et al. (2013)
Baengnyeong and Jeju, Korea	2020	22	190	9.25	4.20	4.85	0.65	ND	103	68.3	ND	Lee et al. (2022)
Gonghe, China	2005	11	321	198	34.3	50.3	–	–	38.4	–	–	Cheng et al. (2007)
Guangzhou, China	2006	17	850	72	185	452	129	20.7	–	–	–	Yang et al. (2008)
Chongyang, China	2013	15	191 ± 107 (47.3–501)	17.1 ± 10.0 (3.65–46.1)	23.6 ± 20.5 (3.33–111)	9.18 ± 6.24 (1.52–25.4)	–	–	133 ± 122 (17.7–479)	–	–	Zhan et al. (2017)
Coastal 7 sites along the Bohai and Yellow Seas, China	2016	24	1,519	666	205	295	29.8	–	236	87.9	–	Yu et al. (2019)
Mohe, Harbin, and Shenzhen, China	2019–2020	19	405	52.8	28.5	7.37	–	0.75	315	–	–	Wang et al. (2023)
Ulaanbaaar, Mongolia	2009	11	433	38.3	252	–	–	–	15.8	–	–	Mamontova et al. (2011)
Nationwide 37 site, Japan	2018	2	163	–	–	–	–	–	104	60	–	Dien et al. (2021)
Cape Hedo, Japan	2009–2014	15	26.3	15 ± 7.8 (4.9–43)	2.5 ± 2.0 (0.7–16)	8.8 ± 11 (1.5–83)	–	–	–	–	–	Takazawa et al. (2016)

ND: Not detected. –: Not included as target compounds.

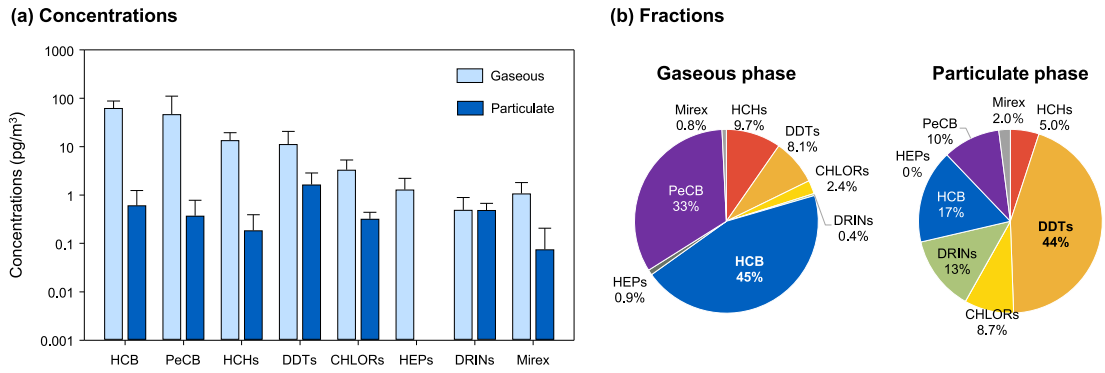

Fig. 3. Levels and patterns of gaseous and particulate OCPs: (a) mean concentrations of OCP groups and (b) fractions of OCP groups in both phases.

(Fig. S3). The dominance of gaseous OCPs is well-documented in previous studies (Wang et al., 2018b, 2023). Most OCPs are predominantly distributed in the gaseous phase due to their high volatility and relatively low log K_{OA} values (e.g., 7.4 for HCB, 6.2 for PeCB, and 7.6 for α-HCH) (Shoeib and Harner, 2009) compared to other POPs, such as polychlorinated biphenyls (PCBs), whose log K_{OA} values range from 8.0 for PCB-28 to 12 for PCB-209 (Harner and Bidleman, 1996). In the gaseous phase, HCB was dominant (62.7 ± 25.1 pg/m^3, 45%), followed by PeCB (46.6 ± 63.5 pg/m^3, 33%), HCHs (13.6 ± 5.79 pg/m^3, 9.7%), DDTs (11.3 ± 9.21 pg/m^3, 8.1%), CHLORs (3.33 ± 1.97 pg/m^3, 2.4%), HEPs (1.30 ± 0.92 pg/m^3, 0.9%), mirex (1.08 ± 0.72 pg/m^3, 0.8%), and DRINs (0.50 ± 0.39 pg/m^3, 0.4%) (Fig. 3b). Legacy OCPs, which have been prohibited, are predominantly found in the gaseous phase, whereas more recently or currently used pesticides (CUPs) are dominant in the particulate phase (Degrendele et al., 2016b) due to their higher log K_{OA} values (e.g., 8.9 for fenpropimorph and 11 for isoproturon) (Götz et al., 2007). In the particulate phase, DDTs were dominant (1.65 ± 1.21 pg/m^3, 44%), followed by HCB (0.61 ± 0.63 pg/m^3, 16%), DRINs (0.49 ± 0.18 pg/m^3, 13%), PeCB (0.37 ± 0.40 pg/m^3, 10%), CHLORs (0.32 ± 0.12 pg/m^3, 8.7%), and HCHs (0.19 ± 0.20 pg/m^3, 5.0%). Consistent with our findings, previous studies have reported high levels of particulate DDTs at urban and background sites in China (Yu et al., 2019), which may be attributed to recent inputs of DDTs (Zhan et al., 2017).

HCB was the most dominant compound in the gaseous phase and the second most abundant in the particulate phase. HCB was commercially used in various applications, including as a fungicide, wood preservative, and intermediate in organic synthesis. It is also unintentionally formed during the production of chlorinated chemicals and various thermal processes (Bailey, 2001). In South Korea, HCB was never registered for agricultural use (Park et al., 2011), but it was found as an impurity in chlorothalonil, with estimated emissions of 77 kg/yr from 1970 to 2004 (Kim et al., 2007). Additionally, domestic HCB emissions from byproducts were estimated to be 245 kg/yr in 2000, with the following source contributions: waste incineration (62%), iron ore sintering (19%), fuel combustion (14%), and non-ferrous metal/mineral production (4%) (Kim et al., 2007). Although HCB was not registered for pesticide use in China, it was historically used in the production of pentachlorophenols (PCPs) (Liu et al., 2009). HCB was found as an impurity in fungicides in China due to a lack of strict regulation. The total production of HCB in China reached 66,000 tonnes between 1988 and 2003, and its production, application, import, and export were prohibited in 2009 (Yu et al., 2019). Due to its extensive historical use, HCB has the potential for re-emission from contaminated soil and water systems (Lin et al., 2012; Qu et al., 2015). In addition, previous studies have reported higher HCB concentrations during colder seasons in China (Qu et al., 2015; Wang et al., 2023), suggesting that combustion sources significantly contribute to HCB levels and indicating the potential for LRAT effects during winter.

PeCB was historically used in chlorobenzene mixtures for PCB products and flame retardants and as an intermediate in the manufacture of pentachloronitrobenzene (Van de Plassche et al., 2001). PeCB can also be released as a byproduct of chlorinated solvent use and from the combustion of solid waste, coal, and biomass (Bailey et al., 2009). Recently, the primary source of PeCB emissions has shifted to unintentional production from activities such as waste incineration and non-ferrous industrial processes (Nielsen et al., 2014). PeCB can be transported over longer distances than other OCPs because of its higher vapor pressure (P_L value of PeCB: 0.30 Pa at 25 °C) compared to other OCPs such as α-HCH (0.22 Pa), TC (6.6 × 10^{-3} Pa), and *p,p'*-DDT (5.0 × 10^{-4} Pa at 25 °C) (Zhang et al., 2009). As a result, PeCB in background regions may be strongly influenced by LRAT due to its high stability (Dien et al., 2021).

Technical HCHs are a mixture of isomers, including α-HCH (60–70%), β-HCH (5–12%), γ-HCH (10–15%), and δ-HCH (6–10%) (Buser and Müller, 1995). Lindane, formerly used as an insecticide, contains over 90% γ-HCH (Walker et al., 1999). In this study, α-HCH was dominant in the gaseous phase (9.65 ± 4.35 pg/m^3, 71%), followed by β-HCH (3.21 ± 2.36 pg/m^3, 21%) and γ-HCH (1.05 ± 0.48 pg/m^3, 7.7%) (Fig. S4a). This profile, with α-HCH dominance, is consistent with that of technical HCHs, suggesting a significant influence from past usage (Shunthirasingham et al., 2010). The higher proportion of β-HCH (21%) observed in this study, compared to its proportion in technical HCHs (5–12%), likely reflects its greater persistence in the environment. Although the half-lives of HCH isomers are similar (Sun et al., 2006), β-HCH has higher chemical and metabolic stability than α-HCH and γ-HCH due to its planar structure (Willett et al., 1998). As β-HCH concentrations decrease more gradually than those of other HCH isomers, its fraction in the atmosphere increases over time (Chakraborty et al., 2010). In contrast, γ-HCH (0.21 ± 0.15 pg/m^3, 90%) was the dominant isomer in the particulate phase (Fig. S4a). The dominance of particulate γ-HCH was also observed in a background area of China (Zhan et al., 2017), indicating a strong influence of lindane use. The mean α/γ-HCH ratios in the gaseous and particulate phases were 9.9 and 0.3, respectively. A high α/γ-HCH ratio typically suggests re-volatilization of technical HCHs (Kalantzi et al., 2001), photochemical conversion of γ-HCH to α-HCH, or biological degradation of γ-HCH (Syed et al., 2013). Previous studies reported mean α/γ-HCH ratios of 0.5 ± 0.3 at a remote site in China (Cheng et al., 2007) and 1.8 at a remote site in Kuwait (Gevao et al., 2018), indicating a stronger influence of lindane use. Conversely, ratios of 12.8 in Greenland (Bossi et al., 2013) and 3.0–6.3 in the Arctic (Baek et al., 2011) suggest re-volatilization of technical HCHs. The α/γ-HCH ratios of daily concentrations in the total phases ranged from 3.6 to 14 (mean: 9.7), similar to other background areas, indicating a significant influence of technical HCHs. When the β-/(α + γ)-HCH ratio is less than 0.5, it indicates recent input from fresh sources (Liu et al., 2012). In this study, the β-/(α + γ)-HCH ratios were 0.3 in the gaseous phase and 0.1 in the particulate phase, suggesting that Deokjeok Island is primarily influenced by more recent emissions, potentially

involving the re-volatilization of technical HCHs from secondary sources.

Technical DDTs were used in South Korea from the 1940s to the early 1970s, with an estimated total application of approximately 2,000 tonnes (Yeo et al., 2004). The environmental release of DDTs from dicofol use was estimated to be 578 kg (KMOE, 2009). However, these amounts are significantly lower than DDT usage for agricultural purposes in other countries, such as China (260,000 tonnes) and India (505, 000 tonnes) (Li and Macdonald, 2005). Both technical DDTs and dicofol formulations contain *p,p'*-DDT as the dominant isomer, but the proportion of *o,p'*-DDT differs between them. Dicofol formulations have a much higher *o,p'*-DDT/*p,p'*-DDT ratio (approximately 7) (Qiu et al., 2005; Shen et al., 2005) compared to technical DDTs (0.2–0.3) (Metcalf, 1955). In this study, the *o,p'*-DDT/*p,p'*-DDT ratios were 1.1 ± 0.4 and 0.4 ± 0.1 in the gaseous and particulate phases, respectively, suggesting that atmospheric DDTs are primarily influenced by the historical use of technical DDTs. Additionally, *o,p'*-DDT was dominant in the gaseous phase (90%), while *p,p'*-DDT was more prevalent in the particulate phase (53%) (Fig. S4b). This result is attributed to the higher vapor pressure of *o,p'*-DDT, which is 7.5 times higher than that of *p,p'*-DDT, leading to its faster volatilization and enrichment in the gaseous phase (Chakraborty et al., 2010). The dominance of *p,p'*-DDE (4.36 ± 3.56 pg/m^3, 38%) in the gaseous phase indicates significant degradation of parent DDTs in the atmosphere. Conversely, *p,p'*-DDT was found in the highest fraction in the particulate phase (0.88 ± 0.67 pg/m^3, 53%), which suggests the presence of fresh DDTs, likely transported from other regions and countries (Chakraborty et al., 2015).

Chlordane was used as a pesticide in South Korea, with an estimated total application of 3 tonnes between 1964 and 1968 (Park et al., 2011), and it was also employed as an adhesive for plywood until 1995 (KMOE, 2009). In the gaseous phase, *cis*-chlordane (CC) was the dominant isomer among CHLORs, accounting for 39%, followed by *trans*-chlordane (TC) (26%), *trans*-nonachlor (TN) (26%), oxychlordane (OxC) (8.9%), and *cis*-nonachlor (CN) (0.8%) (Fig. S4c). In contrast, in the particulate phase, TC (52%) was dominant, followed by CC (28%), TN (19%), and CN (1.2%). TC is more sensitive to photochemical reactions (Bidleman et al., 2002) and is more easily lost in the gaseous phase under increased sunlight exposure (Oehme, 1991). The ratio of *trans/cis*-chlordane (TC/CC) is often used as an indicator of recent chlordane input, with values greater than 1.17 (Daly et al., 2007). In this study, TC/CC ratios ranged from 0.3 to 0.9 in the gaseous phase, indicating historical use and re-emission. In contrast, the higher ratios observed in the particulate phase (1.5–2.4) indicate recent chlordane input. Although TC and CC have similar partitioning and deposition behaviors (Shen and Wania, 2005), the difference in TC/CC ratios between the gaseous and particulate phases likely reflects variations in source proximity and atmospheric persistence. Specifically, the lower TC/CC ratios in the gaseous phase are attributed to the preferential degradation of TC over time, as TC is more volatile than CC (Shen and Wania, 2005). Gaseous CHLORs are significantly influenced by the historical application of technical chlordane, which primarily consists of TC (24%), CC (22%), HEPT (10%), and TN (7%) (Hinckley et al., 1990). The higher TC/CC ratios in the particulate phase may be explained by two factors: (1) the slower degradation of TC in particulate matter and (2) the re-suspension of particulate matter containing higher concentrations and proportions of TC (Jiao et al., 2018). The TC/CC ratios in the particulate phase observed in this study are consistent with those reported in South Korea, ranging from 1.23 to 1.96 in the national POPs monitoring network in 2008 (Park et al., 2011) and from 1.67 to 2.21 at urban and background sites in 2020 (Lee et al., 2022). The annual mean TC/CC ratio in Guangdong Province, South China, was reported at a similar level (2.4 ± 0.5) (Tian et al., 2021), suggesting the influence of recent sources of technical chlordane and heptachlor. These findings indicate a significant influence of LRAT and recent chlordane input in South Korea.

A total of 16,617 tonnes of HEPT were used in South Korea between 1963 and 1979 for agricultural applications and soil pest control (Park et al., 2011). Despite this historically high usage, gaseous HEPT concentrations (0.04 ± 0.11 pg/m^3) were significantly lower than those of its metabolite, HEPX (1.26 ± 0.92 pg/m^3), and neither HEPT nor HEPX was detected in any particulate samples. HEPT residues from past use are easily metabolized into HEPX in the soil (Mackay et al., 2000), which is then re-emitted into the atmosphere, leading to higher HEPX concentrations (Shen et al., 2005). Thus, HEPX may be detected in the atmosphere through volatilization from the soil. Previous studies in South Korea have consistently reported HEPX as the dominant compound, making up over 80% of total HEP concentrations (Park et al., 2011; Khuman et al., 2022).

Endrin and aldrin, which were used in South Korea 30–40 years ago, were not detected in either the gaseous or particulate phases. In contrast, dieldrin was consistently detected in both the gaseous phase (0.50 ± 0.39 pg/m^3) and particulate phase (0.49 ± 0.18 pg/m^3), likely due to its longer half-life of approximately 4–40 years (Mackay et al., 2000). These results align with observations from the national POPs monitoring network (Khuman et al., 2022).

Mirex, which was used for termite control in China, particularly in South China, since 1958 and banned in 2009 (Wang et al., 2010a), has never been registered or used in South Korea (KMOE, 2009), and there is no record of its use in North Korea. Despite no domestic production or usage of mirex, it was detected in over 90% of atmospheric samples, with mean concentrations of 1.08 ± 0.72 pg/m^3 in the gaseous phase and 0.08 ± 0.13 pg/m^3 in the particulate phase. These levels are higher than those reported in other studies (Table 1), providing evidence of ongoing LRAT. Consistent with these results, the national POPs monitoring network also reported the continuous detection of mirex in the atmosphere (Baek et al., 2013; Khuman et al., 2023). Furthermore, elevated mirex levels were observed in the soil of Jiangsu Province, East China (Wang et al., 2010a) and in the atmosphere of the Yangtze River Delta, East China (Zhang et al., 2013), further suggesting the influence of LRAT from continental sources to South Korea.

3.3. Potential source types and source regions

3.3.1. Influence of meteorological parameters

To explore the relationship between OCPs and meteorological parameters, a Spearman correlation analysis was conducted (Table 2). In general, the volatilization of OCPs from surface environments (e.g., water, soil, and vegetation) increases with higher ambient temperatures (Cortes et al., 1998). However, air temperature showed a negative correlation with gaseous Σ_{24} OCPs ($r = -0.39$, $p = 0.26$), though this correlation was not statistically significant, likely due to the small sample size ($n = 10$), which was limited to warmer periods. Conversely, particulate Σ_{24} OCPs and temperature were significantly positively correlated ($r = 0.71$, $p < 0.05$). The most dominant compounds, gaseous HCB and PeCB, exhibited negative correlations with air temperature (HCB: $r = -0.49$, $p = 0.15$; PeCB: $r = -0.41$, $p = 0.24$). A similar negative

Table 2
Correlation coefficients between OCPs and meteorological parameters over the entire sampling period.

	Gaseous phase			Particulate phase		
	Temp	WD	WS	Temp	WD	WS
Σ_{24} OCPs	−0.39	−0.04	0.35	0.71*	−0.58	0.59
HCB	−0.49	0.04	0.04	0.72*	−0.68*	0.70*
PeCB	−0.41	0.09	0.31	0.74*	−0.62	0.67*
HCHs	0.42	−0.25	0.49	0.68*	−0.47	0.61
DDTs	0.72*	−0.33	0.77**	0.71*	−0.43	0.55
CHLORs	0.18	−0.13	0.37	0.17	−0.59	0.12
HEPs	−0.42	−0.38	0.05	–	–	–
DRINs	0.13	0.49	0.29	0.36	−0.33	0.20
Mirex	0.68*	−0.27	0.83**	0.23	−0.31	0.46

*Correlation is significant at the 0.05 level (2-tailed).
**Correlation is significant at the 0.01 level (2-tailed).

correlation between HCB and temperature was observed in a study conducted in Lijiang, China (Gong et al., 2018), which was attributed to incomplete combustion sources (Liu et al., 2009). A previous study in China reported elevated OCP levels during spring due to the influence of combustion sources (Yu et al., 2019). Therefore, combustion may have contributed to the observed peaks in HCB and PeCB concentrations, as well as the negative correlation between gaseous Σ_{24} OCPs and temperature. On the other hand, particulate HCB and PeCB were positively correlated with temperature (HCB: $r = 0.72$, $p < 0.05$; PeCB: $r = 0.74$, $p < 0.05$), likely due to LRAT of particulate matter containing high levels of OCPs during the summer (Ya et al., 2019). Most other OCPs, except HEPs, also showed positive correlations with temperature in both the gaseous and particulate phases, largely driven by temperature-induced volatilization from surface environments. For example, DDTs in the gaseous ($r = 0.72$, $p < 0.05$) and particulate ($r = 0.71$, $p < 0.05$) phases were significantly correlated with temperature. Similarly, significant correlations were found for gaseous mirex ($r = 0.68$, $p < 0.05$) and particulate HCHs ($r = 0.68$, $p < 0.05$), indicating strong evidence of re-emission from past use. However, no significant correlation of CHLORs and DRINs with temperature suggests that they were substantially influenced by both local emissions and external inputs (Yu et al., 2019).

To assess the temperature dependence of individual OCPs, the Clausius-Clapeyron (*CC*) equation was applied to temperature and OCP concentration data, yielding regression coefficients and ΔH_{sa} values (Sofuoglu et al., 2004). A detailed description of the *CC* equation is provided in Text S4. The ΔH_{sa} values were calculated to help identify major sources, indicating the potential for LRAT or re-volatilization from local sources (Wania et al., 1998). Both *o,p'*-DDT and *p,p'*-DDT exhibited strong temperature dependence ($R^2 > 0.7$) and had high ΔH_{sa} values (2,416 and 1,299 J/mol, respectively) (Table S4), suggesting that re-emission from local sources is the dominant source. This finding aligns with the DDT diagnostic ratios discussed in Section 3.2, which point to the re-volatilization of technical DDT as the primary source of DDTs. Other compounds such as *o,p'*-DDD, *p,p'*-DDE, *p,p'*-DDD, CN, and mirex showed moderate temperature dependence (R^2 between 0.4 and 0.7), suggesting their persistence in surface media (e.g., soil and water) and subsequent volatilization under high-temperature conditions. Notably, relatively high ΔH_{sa} values were estimated for *o,p'*-DDD (2,130 J/mol), *p,p'*-DDD (2,258 J/mol), *o,p'*-DDE (1,271 J/mol), and mirex (1,223 J/mol), indicating that these compounds are predominantly re-emitted from past use. Other OCPs, such as HCHs, CC, TC, TN, OxC, HEPs, dieldrin, HCB, and PeCB, showed relatively shallow slopes and lower R^2 values (<0.4), indicating low-temperature dependence and suggesting influences from both LRAT and newer emission sources. Additionally, CHLORs, dieldrin, HCB, and PeCB had low ΔH_{sa} values (240–655, 203, −555, and −1,764 J/mol, respectively), indicating a significant influence of LRAT. In particular, as mentioned above, fresh sources (e.g., unintentional emissions) of HCB and PeCB have been identified (Yu et al., 2019; Wang et al., 2023).

The relationships between wind patterns and OCP concentrations were also investigated. The daily mean wind direction ranged from 157° to 297° (Fig. S1), with predominant westerly and southerly winds during the sampling period. Westerly and northwesterly winds at the sampling site suggest LRAT from Northeast Asia to the Korean Peninsula. Although southerly winds were dominant on several days (e.g., May 22, July 28, and July 29), air masses originated from distant areas, including North and South China (Fig. S1). Particulate OCPs had negative correlations with wind direction (e.g., HCB: $r = -0.68$, $p < 0.05$), suggesting that southerly winds, likely coming from China, were associated with higher OCP concentrations. In contrast, gaseous OCPs displayed relatively weak positive or negative correlations with wind direction, implying influence from various source regions. A strong correlation between air pollutants and wind speed indicates the influence of LRAT, while a weak correlation denotes emissions from local sources (Hillery et al., 1997). Most OCPs were positively correlated with wind speed, indicating a significant influence of LRAT. Specifically, gaseous DDTs and mirex ($p < 0.01$) and particulate HCB and PeCB ($p < 0.05$) were significantly correlated with wind speed. Other OCPs, which were less correlated with wind speed, were likely influenced by both LRAT and local emissions (Yu et al., 2019).

3.3.2. Potential source areas

To identify the potential source regions of OCPs, a backward air trajectory analysis was performed. The daily backward trajectories during the HiVol sampling period were grouped into two clusters (Fig. S5). Cluster 1 indicated the influence of LRAT from North China, specifically from Hebei and Inner Mongolia provinces, as well as Northeast China (Liaoning province). Cluster 2, which represented the dominant air mass (63%), originated from East China, particularly from Shanghai and Jiangsu provinces. The LRAT of air masses from industrial regions in North and East China to South Korea, even during summer, is well documented (Jeong et al., 2011; Lee et al., 2022).

The CWT maps were separately generated for both gaseous and particulate Σ_{24} OCPs (Fig. 4). The CWT results for gaseous OCPs suggest that East China is a potential source region (Fig. 4a). The levels of HCB and PeCB at the sampling site were likely influenced primarily by emissions from Shandong and Jiangsu provinces in East China and Hebei province in North China. HCB has never been registered as a pesticide for agricultural purposes in China, but it was predominantly used in the production of PCP and PCP-Na (Liu et al., 2009). After its regulation in 1983, HCB production decreased drastically and continued only in Tianjin until 2009 (Wang et al., 2010b). Despite the ban, unintended emissions of HCB have occurred due to its presence as an impurity in pesticides, chlorine-related manufacturing, and combustion processes, resulting in significant accumulation in northern China (Wang et al., 2023). In addition, biomass combustion for heating was identified as an important local source of HCB in North and Northeast China (Qu et al., 2015). The CWT plots for both gaseous and particulate HCB (Fig. S6) are consistent with the distribution patterns of primary HCB emissions in China.

Potential source areas for HCHs, DDTs, CHLORs, DRINs, and HEPs were identified in East China (Shandong and Jiangsu provinces), North China (Hebei and Inner Mongolia provinces), and Northeast China (Liaoning province) (Fig. S6). National soil monitoring in China reported high concentrations of DDTs and HCHs in North and Northeast China (Yu et al., 2020). These results demonstrate the grasshopping effects of OCPs, which lead to their accumulation in northern China (Wang et al., 2023). OCPs were heavily used in South, Central, and East China, while Northeast China is considered a recent sink region for OCPs due to the slower biodegradation in colder climates (Wang et al., 2023). A previous modeling study also reported that the outflow of banned OCPs from China occurs mainly through Northeast China (Heilongjiang and Jilin provinces) and North China (Inner Mongolia province), particularly during the summer (Tian et al., 2009), which is consistent with the hotspots identified in the CWT maps. Furthermore, high mirex concentrations in Liaoning province soils (5–20 pg/g) were reported (Wang et al., 2010a), supporting the CWT result of this study. Overall, the CWT maps for gaseous OCPs effectively identified potential source areas for the re-emission of accumulated OCPs from the soil.

For particulate OCPs, the CWT results revealed that primary source regions included North China (Beijing, Hebei, and Shandong provinces) and Northeast China (Liaoning province) (Fig. 4b). Notably, the CWT maps for each OCP group, except for mirex, showed similar patterns to the CWT map for Σ_{24} OCPs (Fig. S6). A previous study reported the highest levels of particulate HCB and DDTs in the East China Sea during the summer (Ya et al., 2019), suggesting possible inflow from China to South Korea across the Yellow Sea in warm seasons. In addition, potential source areas for particulate mirex were identified in East China (Anhui and Jiangsu provinces), where it was historically used for termite control (Wang et al., 2010a). The CWT plots for particulate OCPs emphasized the influence of LRAT, along with fresh OCP emissions.

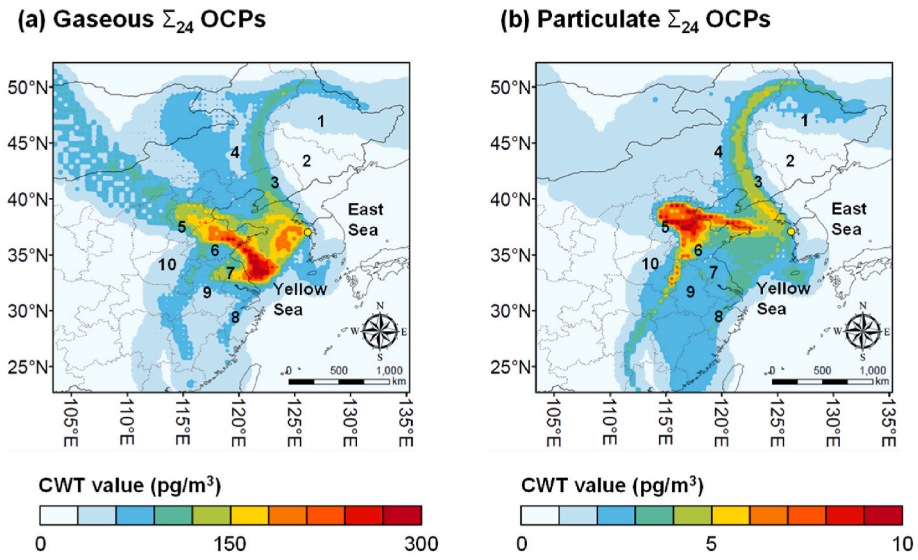

Fig. 4. CWT results for (a) gaseous and (b) particulate Σ_{24} OCPs. The numbers correspond to 10 provinces in China: (1) Heilongjiang, (2) Jilin, (3) Liaoning, (4) Inner Mongolia, (5) Hebei, (6) Shandong, (7) Jiangsu, (8) Zhejiang, (9) Anhui, and (10) Henan.

3.4. G/P partitioning behavior

Among the 24 target OCPs, 13 OCPs detected in both the particulate and gaseous phases were used for the G/P partitioning analysis. Two types of nonlinear regression analyses for the Junge-Pankow model were conducted using experimentally determined G/P partitioning data (Fig. S7). The two-parameter model consistently showed higher correlation coefficients than the one-parameter model, which assumes G/P equilibrium with a theoretical slope ($m = -1$). The slope values (m) in May (mean: −0.68) were closer to −1 than those in July ($m = -7.98$) (Table S5), suggesting a closer equilibrium state in May. Notably, the curves for May 22 and 23 shifted to the lower left compared to other days in May and July, indicating an increased contribution of gaseous OCPs. On these days, gaseous OCP concentrations were highest (270 and 323 pg/m^3), while particulate concentrations were lower (1.70 and 1.67 pg/m^3), reflecting enhanced re-emissions of historically accumulated OCPs. The PM_{10} concentrations on May 22 (36.4 μg/m^3) and May 23 (38.6 μg/m^3) were also lower than on other sampling days (mean: 75.6 μg/m^3), indicating a low influx of particulate matter and suggesting an equilibrium state. Interestingly, the shallow S-curves observed on May 24–26 had higher slope values (m: −0.61, −0.45, and −0.57). During this period, high particulate fractions of OCPs ($\log P_L > -3$), such as TC, CC, TN, *p,p'*-DDD, and *p,p'*-DDE, were observed, along with relatively high PM_{10} concentrations (mean: 81.2 μg/m^3) compared to May 22–23 (37.5 μg/m^3). Although Σ_{24} OCP concentrations in the total phase were relatively low on May 24–26, the particulate concentrations of these compounds remained consistent with levels observed on other days, resulting in the highest particulate fractions. This result indicates a continuous influence of LRAT. In addition, July samples with high particulate Σ_{24} OCP concentrations exhibited lower slope values (m: −1.11 to −4.70), suggesting a stronger disequilibrium between the gaseous and particulate phases in July, when relatively high PM_{10} concentrations (mean: 72.2 μg/m^3) were observed. This finding aligns with a previous study suggesting that the transport of aerosols, along with high PM concentrations and dust incursions, may contribute to the disequilibrium (Iakovides et al., 2021).

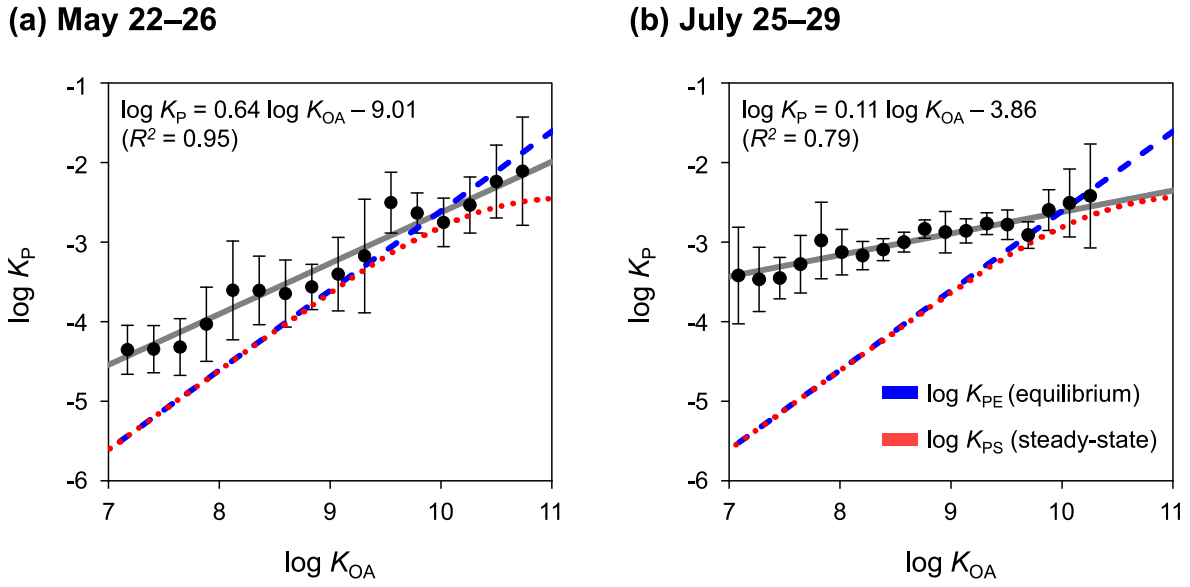

Fig. 5. Regression plots showing the relationship between log K_{OA} and log K_P, log K_{PE}, and log K_{PS} for 13 individual OCPs in (a) May and (b) July. The log K_P values represent the measured data, while the K_{PE} and K_{PS} values were predicted using the K_{OA} and steady-state models, respectively.

Further examination of the relationship between log K_P and log K_{OA} was conducted using the K_{OA} absorption model and the steady-state model (Li et al., 2015). The coefficients of determination (R^2) between log K_P and log K_{OA} values were 0.95 and 0.79 ($p < 0.01$) for May and July, respectively (Fig. 5). The slope of the regression line in May (0.64) was much closer to 1 than the slope in July (0.11). This result indicates a substantial difference in the G/P partitioning of OCPs between the measured log K_p in July and the predicted value from the equilibrium model (log K_{PE}) (Harner and Bidleman, 1998). The steady-state model (log K_{PS}) also showed a considerable difference from the regression line for July, only matching well with log K_{OA} values greater than 10 (Fig. 5b). This phenomenon has been reported in previous studies; for instance, model predictions deviate from measured K_P when log K_{OA} is below 11.4 in a cross-regional study in China (Wang et al., 2023), and a low regression slope was observed in the Antarctic (slope: 0.24) when strong LRAT influences were present (Wang et al., 2018b). These findings suggest that particulate OCP input plays an important role in OCP partitioning. The steady-state model, which takes into account a non-equilibrium term (log α), showed a gradual decrease in the slope for log K_{OA} values above 10, influenced by the wet and dry deposition of particles (Qiao et al., 2019). The regression line for May is closer to the equilibrium model result for log $K_{OA} > 10$, indicating stable equilibrium conditions for OCPs. Conversely, the regression line for July is much closer to the steady-state model result for log $K_{OA} > 10$, suggesting enhanced particle deposition in July (Li et al., 2015). Consequently, the G/P partitioning models indicate that gaseous OCP emissions in May lead to equilibrium, whereas particulate OCP inputs contributed to the deviations from equilibrium observed in July, which had higher PM_{10} concentrations (mean: 72.2 μg/m^3) than in May (mean: 59.7 μg/m^3). Previous studies have similarly reported that an influx of particulate matter resulted in disequilibrium (Wang et al., 2018b; Qiao et al., 2019). The predicted particle-bound fraction was notably underestimated in July compared to May when log $K_{OA} < 10$, suggesting the influence of additional factors. Previous studies reported sampling artifacts and the sorption of compounds with relatively high vapor pressures onto other sorbents as contributors to disequilibrium conditions (Melymuk et al., 2016; Wang et al., 2018a). These factors likely account for the discrepancies observed in July between the measured and predicted data.

3.5. Air-soil gas exchange

Air and soil fugacity fractions for 12 OCPs detected in both PUF-PAS and soil samples are presented in Fig. 6. Theoretically, fugacity fractions between 0.3 and 0.7 suggest equilibrium, with a 20% margin of error (Harner et al., 2001). PeCB exhibited a mean fugacity fraction above 0.7, indicating net volatilization from soil to air. This result implies that soil remains a source of PeCB to the atmosphere due to its historical use and accumulation in soil. The ΔH_{sa} values derived from the *CC* equation further support the strong volatilization of PeCB from soil. This finding is consistent with observations in background areas of Hungary (Degrendele et al., 2016a). Meanwhile, HCB, α-HCH, TC, CC, and dieldrin exhibited tendencies close to equilibrium between air and soil. However, TC (0.03–0.95) and CC (0.01–0.86) displayed a wide range of fugacity fractions, reflecting their ongoing dynamic behavior in the environment. Lower fugacity fractions (<0.3) observed for β-HCH, DDTs, TN, and HEPX suggest that net deposition from air to soil is the dominant process. Since there are no new emissions of these banned OCPs, their presence in the study area is likely a result of LRAT followed by deposition. A previous study in the Tibetan background region reported a similar fate for DDTs, showing LRAT and deposition (Wang et al., 2012).

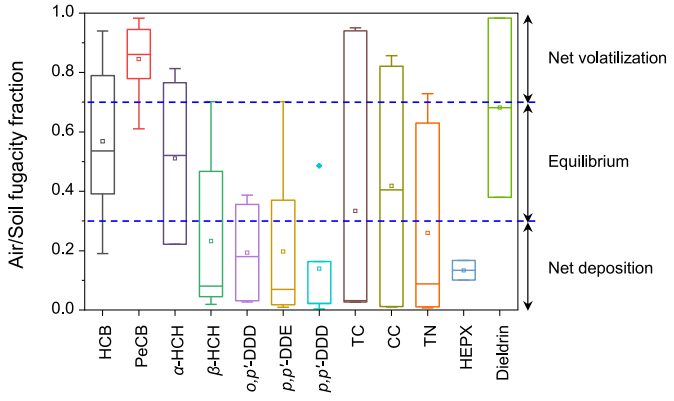

Fig. 6. Box plots showing the air/soil fugacity fractions of 12 OCPs detected in both PUF-PAS and soil samples.

3.6. Limitations and implications

In this study, short-term monitoring was the only feasible option due to the geographical constraints of the remote island, and the samples were collected in 2013, reflecting a relatively outdated pollution status. However, in our previous study, nationwide annual and seasonal variations in OCP levels, profiles, and potential sources remained relatively consistent between 2008 and 2017 (Khuman et al., 2023). Therefore, the potential sources and the influence of LRAT of OCPs identified in this study likely reflect the conditions in background areas of the Korean Peninsula, particularly near the west coast, during warm periods. Additionally, the relatively stable long-term trends in OCP concentrations in South Korea suggest that the sources and environmental fate of OCPs, including air-soil exchange, have remained largely unchanged over the past decade. Furthermore, slight decreases in α-HCH and γ-HCH concentrations, along with increases in *o,p'*-DDE and HCB concentrations, were observed in China (Wang et al., 2018a). Since OCPs have been extensively used in South and East China (Wang et al., 2023) and persist for long periods in soil and water, they are continually re-emitted into the atmosphere (Chen et al., 2023). As a result, the annual trends and source regions of OCPs transported from China are expected to have remained consistent during the study period and in recent years.

4. Conclusion

This study investigated the influence of LRAT on the levels and patterns of OCPs on Deokjeok Island, a background site in South Korea. The total (Σ_{24}) OCP concentrations were lower than those observed in the national POPs monitoring network of South Korea and other Northeast Asian countries. Gaseous OCP concentrations, particularly the higher levels of HCB and PeCB, were linked to the past usage of technical HCHs and DDTs, indicating that atmospheric OCP levels are influenced by volatilization from surface environments. In contrast, particulate OCPs, dominated by DDTs, likely originated from recent emissions and atmospheric transport. The detection of mirex, which has never been used in South Korea, in both gaseous and particulate phases provides evidence of LRAT influence. In addition, significant influences of LRAT on DDTs were identified through the *CC* equation and strong correlations with wind speed. The primary source regions for the LRAT of gaseous OCPs to South Korea were identified as East, North, and Northeast China, along with re-emissions of accumulated OCPs from soil. CWT maps for particulate OCPs highlighted fresh inputs, with Beijing, Hebei, Tianjin, and Shandong identified as key source regions. Secondary emissions from historically accumulated OCPs on surfaces may contribute to elevated gaseous concentrations, potentially leading to G/P equilibrium. In contrast, the fresh input of particulate OCPs, likely associated with high PM concentrations, contributed to non-equilibrium conditions. Fugacity fractions suggested equilibrium or net deposition between air and soil for most OCPs, except for PeCB, indicating ongoing cycling, potential LRAT, and subsequent deposition. The results of this study suggest that LRAT continues to significantly influence atmospheric OCP concentrations in South Korea, with ongoing

re-emissions. Based on the various monitoring and modeling tools used in this study, it is recommended to conduct long-term seasonal monitoring and modeling of both OCPs and CUPs to further evaluate the impacts of LRAT and local emissions.

CRediT authorship contribution statement

Ho-Young Lee: Writing – original draft, Methodology, Formal analysis. **Sung-Deuk Choi:** Writing – review & editing, Supervision, Project administration. **Min-Kyu Park:** Formal analysis. **Yoon-Se Lee:** Formal analysis. **Chul-Su Kim:** Formal analysis. **Cheol-Hee Kim:** Project administration. **Lim-Seok Chang:** Resources.

Declaration of competing interest

The authors declare that they have no known competing financial interests or personal relationships that could have appeared to influence the work reported in this paper.

Acknowledgments

This study was supported by the National Research Foundation of Korea (NRF) (RS-2023-00209329), the 2019 Research Fund (1.190101.01) of Ulsan National Institute of Science and Technology (UNIST), and the National Institute of Environmental Research (NIER-SP2013-18).

Appendix A. Supplementary data

Supplementary data to this article can be found online at https://doi.org/10.1016/j.chemosphere.2024.143964.

Data availability

No data was used for the research described in the article.

References

Angulo Lucena, R., Farouk Allam, M., Serrano Jiménez, S., Luisa Jodral Villarejo, M., 2007. A review of environmental exposure to persistent organochlorine residuals during the last fifty years. Curr. Drug Saf. 2, 163–172.
Baek, S.-Y., Choi, S.-D., Chang, Y.-S., 2011. Three-year atmospheric monitoring of organochlorine pesticides and polychlorinated biphenyls in polar regions and the South Pacific. Environ. Sci. Technol. 45, 4475–4482.
Baek, S.-Y., Jurng, J.S., Chang, Y.-S., 2013. Spatial distribution of polychlorinated biphenyls, organochlorine pesticides, and dechlorane plus in Northeast Asia. Atmos. Environ. 64, 40–46.
Bailey, R.E., 2001. Global hexachlorobenzene emissions. Chemosphere 43, 167–182.
Bailey, R.E., Van Wijk, D., Thomas, P.C., 2009. Sources and prevalence of pentachlorobenzene in the environment. Chemosphere 75, 555–564.
Bidleman, T.F., Jantunen, L.M.M., Helm, P.A., Brorström-Lundén, E., Juntto, S., 2002. Chlordane enantiomers and temporal trends of chlordane isomers in Arctic air. Environ. Sci. Technol. 36, 539–544.
Bossi, R., Skjøth, C.A., Skov, H., 2013. Three years (2008-2010) of measurements of atmospheric concentrations of organochlorine pesticides (OCPs) at Station Nord, North-East Greenland. Environ. Sci.-Proc. Imp. 15, 2213–2219.
Buser, H.R., Müller, M.D., 1995. Isomer and enantioselective degradation of hexachlorocyclohexane isomers in sewage sludge under anaerobic conditions. Environ. Sci. Technol. 29, 664–672.
Chakraborty, P., Zhang, G., Li, J., Sivakumar, A., Jones, K.C., 2015. Occurrence and sources of selected organochlorine pesticides in the soil of seven major Indian cities: assessment of air-soil exchange. Environ. Pollut. 204, 74–80.
Chakraborty, P., Zhang, G., Li, J., Xu, Y., Liu, X., Tanabe, S., Jones, K.C., 2010. Selected organochlorine pesticides in the atmosphere of major Indian cities: levels, regional versus local variations, and sources. Environ. Sci. Technol. 44, 8038–8043.
Chen, L., Qian, Y., Jia, Q., Weng, R., Zhang, X., Li, Y., Qiu, J., 2023. A national-scale distribution of organochlorine pesticides (OCPs) in cropland soils and major types of food crops in China: co-occurrence and associated risks. Sci. Total Environ. 861, 160637.
Cheng, H., Zhang, G., Jiang, J.X., Li, X., Liu, X., Li, J., Zhao, Y., 2007. Organochlorine pesticides, polybrominated biphenyl ethers and lead isotopes during the spring time at the Waliguan Baseline Observatory, northwest China: implication for long-range atmospheric transport. Atmos. Environ. 41, 4734–4747.
Choi, S.-D., 2014. Time trends in the levels and patterns of polycyclic aromatic hydrocarbons (PAHs) in pine bark, litter, and soil after a forest fire. Sci. Total Environ. 470, 1441–1449.
Cortes, D.R., Basu, I., Sweet, C.W., Brice, K.A., Hoff, R.M., Hites, R.A., 1998. Temporal trends in gas-phase concentrations of chlorinated pesticides measured at the shores of the Great Lakes. Environ. Sci. Technol. 32, 1920–1927.
Daly, G.L., Lei, Y.D., Teixeira, C., Muir, D.C.G., Castillo, L.E., Jantunen, L.M.M., Wania, F., 2007. Organochlorine pesticides in the soils and atmosphere of Costa Rica. Environ. Sci. Technol. 41, 1124–1130.
Degrendele, C., Audy, O., Hofman, J., Kucerik, J., Kukucka, P., Mulder, M.D., Pribylová, P., Prokes, R., Sánka, M., Schaumann, G.E., Lammel, G., 2016a. Diurnal variations of air-soil exchange of semivolatile organic compounds (PAHs, PCBs, OCPs, and PBDEs) in a Central European receptor area. Environ. Sci. Technol. 50, 4278–4288.
Degrendele, C., Okonski, K., Melymuk, L., Landlová, L., Kukučka, P., Audy, O., Kohoutek, J., Čupr, P., Klánová, J., 2016b. Pesticides in the atmosphere: a comparison of gas-particle partitioning and particle size distribution of legacy and current-use pesticides. Atmos. Chem. Phys. 16, 1531–1544.
Dien, N.T., Hirai, Y., Koshiba, J., Sakai, S.I., 2021. Factors affecting multiple persistent organic pollutant concentrations in the air above Japan: a panel data analysis. Chemosphere 277, 130356.
Ding, Y., Huang, H., Chen, W., Zhang, Y., Chen, W., Xing, X., Qi, S., 2022. Background levels of OCPs, PCBs, and PAHs in soils from the eastern Pamirs, China, an alpine region influenced by westerly atmospheric transport. J. Environ. Sci. 115, 453–464.
Draxler, R., Stunder, B., Rolph, G., Stein, A., Taylor, A., 2020. HYSPLIT user's guide version 5. Air Resources Laboratory. National Oceanic and Atmospheric Administration, USA.
Gevao, B., Porcelli, M., Rajagopalan, S., Krishnan, D., Martinez-Guijarro, K., Alshemmari, H., Bahloul, M., Zafar, J., 2018. Spatial and temporal variations in the atmospheric concentrations of "Stockholm Convention" organochlorine pesticides in Kuwait. Sci. Total Environ. 622, 1621–1629.
Gong, P., Wang, X., Sheng, J., Wang, H., Yuan, X., He, Y., Qian, Y., Yao, T., 2018. Seasonal variations and sources of atmospheric polycyclic aromatic hydrocarbons and organochlorine compounds in a high-altitude city: evidence from four-year observations. Environ. Pollut. 233, 1188–1197.
Gong, P., Wang, X., Sheng, J., Yao, T., 2010. Variations of organochlorine pesticides and polychlorinated biphenyls in atmosphere of the Tibetan Plateau: role of the monsoon system. Atmos. Environ. 44, 2518–2523.
Götz, C.W., Scheringer, M., Macleod, M., Roth, C.M., Hungerbühler, K., 2007. Alternative approaches for modeling gas-particle partitioning of semivolatile organic chemicals: model development and comparison. Environ. Sci. Technol. 41, 1272–1278.
Harner, T., Bidleman, T.F., 1996. Measurements of octanol-air partition coefficients for polychlorinated biphenyls. J. Chem. Eng. Data 41, 895–899.
Harner, T., Bidleman, T.F., 1998. Octanol-air partition coefficient for describing particle/gas partitioning of aromatic compounds in urban air. Environ. Sci. Technol. 32, 1494–1502.
Harner, T., Bidleman, T.F., Jantunen, L.M.M., Mackay, D., 2001. Soil-air exchange model of persistent pesticides in the United States cotton belt. Environ. Toxicol. Chem. 20, 1612–1621.
Hillery, B.R., Basu, I., Sweet, C.W., Hites, R.A., 1997. Temporal and spatial trends in a long-term study of gas-phase PCB concentrations near the Great Lakes. Environ. Sci. Technol. 31, 1811–1816.
Hinckley, D.A., Bidleman, T.F., Foreman, W.T., Tuschall, J.R., 1990. Determination of vapor pressures for nonpolar and semipolar organic compounds from gas chromatographic retention data. J. Chem. Eng. Data 35, 232–237.
Hippelein, M., McLachlan, M.S., 1998. Soil/air partitioning of semivolatile organic compounds. 1. Method development and influence of physical− chemical properties. Environ. Sci. Technol. 32, 310–316.
Iakovides, M., Apostolaki, M., Stephanou, E.G., 2021. PAHs, PCBs and organochlorine pesticides in the atmosphere of Eastern Mediterranean: investigation of their occurrence, sources and gas-particle partitioning in relation to air mass transport pathways. Atmos. Environ. 244, 117931.
Jaward, F.M., Zhang, G., Nam, J.J., Sweetman, A.J., Obbard, J.P., Kobara, Y., Jones, K.C., 2005. Passive air sampling of polychlorinated biphenyls, organochlorine compounds, and polybrominated diphenyl ethers across Asia. Environ. Sci. Technol. 39, 8638–8645.
Jeong, U.K., Kim, J., Lee, H.L., Jung, J.S., Kim, Y.J., Song, C.H., Koo, J.-H., 2011. Estimation of the contributions of long range transported aerosol in East Asia to carbonaceous aerosol and PM concentrations in Seoul, Korea using highly time resolved measurements: a PSCF model approach. J. Environ. Monit. 13, 1905–1918.
Jiao, L., Lao, Q., Chen, L., Chen, F., Sun, X., Zhao, M., 2018. Concentration and influence factors of organochlorine pesticides in atmospheric particles in a coastal island in Fujian, Southeast China. Aerosol Air Qual. Res. 18, 2982–2996.
Jin, G.-Z., Kim, S.-M., Lee, S.-Y., Park, J.-S., Kim, D.-H., Lee, M.-J., Sim, K.-T., Kang, H.-G., Kim, I.-G., Shin, S.-K., Seok, K.-S., Hwang, S.-R., 2013. Levels and potential sources of atmospheric organochlorine pesticides at Korea background sites. Atmos. Environ. 68, 333–342.
Kalantzi, O.I., Alcock, R.E., Johnston, P.A., Santillo, D., Stringer, R.L., Thomas, G.O., Jones, K.C., 2001. The global distribution of PCBs and organochlorine pesticides in butter. Environ. Sci. Technol. 35, 1013–1018.
Kallenborn, R., Christensen, G., Evenset, A., Schlabach, M., Stohl, A., 2007. Atmospheric transport of persistent organic pollutants (POPs) to Bjørnøya (Bear Island). J. Environ. Monit. 9, 1082–1091.
Kang, J.-H., Park, H.K., Chang, Y.-S., Choi, J.-W., 2008. Distribution of organochlorine pesticides (OCPs) and polychlorinated biphenyls (PCBs) in human serum from urban areas in Korea. Chemosphere 73, 1625–1631.

Khuman, S.N., Park, M.-K., Kim, H.-J., Hwang, S.-M., Lee, C.-H., Choi, S.-D., 2022. Organochlorine pesticides in the urban, suburban, agricultural, and industrial soil in South Korea after three decades of ban: spatial distribution, sources, time trend, and implicated risks. Environ. Pollut. 311, 119938.
Khuman, S.N., Park, M.-K., Kim, H.-J., Hwang, S.-M., Lee, C.-H., Choi, S.-D., 2023. Nationwide assessment of atmospheric organochlorine pesticides over a decade during 2008-2017 in South Korea. Sci. Total Environ. 877, 162927.
Kim, S.-K., Khim, J.S., Lee, K.-T., Giesy, J.P., Kannan, K., Lee, D.-S., Koh, C.-H., 2007. Emission, contamination and exposure, fate and transport, and national management strategy of persistent organic pollutants in South Korea. Dev. Environ. Sci. 7, 31–157.
Kirchner, M., Jakobi, G., Körner, W., Levy, W., Moche, W., Niedermoser, B., Schaub, M., Ries, L., Weiss, P., Antritter, F., Fischer, N., Henkelmann, B., Schramm, K.-W., 2016. Ambient air levels of organochlorine pesticides at three high alpine monitoring stations: trends and dependencies on geographical origin. Aerosol Air Qual. Res. 16, 738–751.
Korea Ministry of Environment (KMOE), 2009. Evaluation of the National POPs Contamination Status 2008. South Korea.
Korea Ministry of Environment (KMOE), 2015. 2010~2013 Result Report of Persistent Organic Pollutants Monitoring Network. South Korea.
Korea Ministry of Environment (KMOE), 2017. 2014~2016 Result Report of Persistent Organic Pollutants Monitoring Network. South Korea.
Korea Ministry of Environment (KMOE), 2018. 2017 Result Report of Persistent Organic Pollutants Monitoring Network. South Korea.
Lee, M.S., Lee, S.M., Noh, S., Park, K.-S., Yu, S.-M., Lee, S.H., Do, Y.-S., Kim, Y.-H., Kwon, M.H., Kim, H.J., Park, M.-K., 2022. Assessment of organochlorine pesticides in the atmosphere of South Korea: spatial distribution, seasonal variation, and sources. Environ. Monit. Assess. 194, 754.
Li, Y., Lohmann, R., Zou, X., Wang, C., Zhang, L., 2020. Air-water exchange and distribution pattern of organochlorine pesticides in the atmosphere and surface water of the open Pacific Ocean. Environ. Pollut. 265, 114956.
Li, Y.F., Ma, W.L., Yang, M., 2015. Prediction of gas/particle partitioning of polybrominated diphenyl ethers (PBDEs) in global air: a theoretical study. Atmos. Chem. Phys. 15, 1669–1681.
Li, Y.F., Macdonald, R.W., 2005. Sources and pathways of selected organochlorine pesticides to the Arctic and the effect of pathway divergence on HCH trends in biota: a review. Sci. Total Environ. 342, 87–106.
Lin, T., Li, J., Xu, Y., Liu, X., Luo, C., Cheng, H., Chen, Y., Zhang, G., 2012. Organochlorine pesticides in seawater and the surrounding atmosphere of the marginal seas of China: spatial distribution, sources and air-water exchange. Sci. Total Environ. 435, 244–252.
Liu, J., Wang, H.-Y., Song, S.-J., Ma, H.-C., Sun, W.-T., Wang, L., Wang, Y., Yi, X.-L., Guo, L.-Q., Li, P.-H., 2019. Levels, potential sources and risk assessment of organochlorine pesticides in atmospheric particulate matter at regional background site. Aerosol Air Qual. Res. 19, 2008–2016.
Liu, W.-X., He, W., Qin, N., Kong, X.-Z., He, Q.-S., Ouyang, H.-L., Yang, B., Wang, Q.-M., Yang, C., Jiang, Y.-J., Wu, W.-J., Xu, F.-L., 2012. Residues, distributions, sources, and ecological risks of OCPs in the water from Lake Chaohu, China. Sci. World J. 2012, 897697.
Liu, X., Zhang, G., Li, J., Yu, L.-L., Xu, Y., Li, X.-D., Kobara, Y., Jones, K.C., 2009. Seasonal patterns and current sources of DDTs, chlordanes, hexachlorobenzene, and endosulfan in the atmosphere of 37 Chinese cities. Environ. Sci. Technol. 43, 1316–1321.
Mackay, D., Shiu, W.Y., Ma, K.C., 2000. Physico-Chemical Properties and Environmental Fate - Handbook. Chapman and Hall/CRCnetBase, England.
Mamontova, E.A., Tarasova, E.N., Ganchimeg, D., Kuzmin, M.I., Mamontov, A.A., Khomutova, M.Y., Burmaa, G., Odontuya, G., Erdenebayasgalan, G., 2011. Persistent organic pollutants (PCBs and OCP) in air and soil from Ulaanbaatar and the Lake Hovsgol region, Mongolia. Mong. J. Chem. 12, 69–77.
Mamontova, E.A., Tarasova, E.N., Mamontov, A.A., Goreglyad, A.V., Tkachenko, L.L., 2019. Variations in the concentration of polychlorinated biphenyls and organochlorine pesticides in air over the Northern Hovsgol Region in 2008–2015. Russ. Meteorol. Hydrol. 44, 78–85.
Mao, S., Zhang, G., Li, J., Geng, X., Wang, J., Zhao, S., Cheng, Z., Xu, Y., Li, Q., Wang, Y., 2020. Occurrence and sources of PCBs, PCNs, and HCB in the atmosphere at a regional background site in east China: implications for combustion sources. Environ. Pollut. 262, 114267.
Melymuk, L., Bohlin-Nizzetto, P., Prokeš, R., Kukučka, P., Klánová, J., 2016. Sampling artifacts in active air sampling of semivolatile organic contaminants: comparing theoretical and measured artifacts and evaluating implications for monitoring networks. Environ. Pollut. 217, 97–106.
Metcalf, R.L., 1955. Physiological basis for insect resistance to insecticides. Physiol. Rev. 35, 197–232.
Nielsen, O.-K., Plejdrup, M.S., Winther, M., Nielsen, M., Fauser, P., Mikkelsen, M.H., Albrektsen, R., Hjelgaard, K., Hoffmann, L., Thomsen, M., 2014. Danish Emission Inventory for Hexachlorobenzene and Polychlorinated Biphenyls. Danish Centre for Environment and Energy, Denmark.
Odabasi, M., Cetin, B., 2012. Determination of octanol-air partition coefficients of organochlorine pesticides (OCPs) as a function of temperature: application to air-soil exchange. J. Environ. Manag. 113, 432–439.
Oehme, M., 1991. Further evidence for long-range air transport of polychlorinated aromates and pesticides: north America and Eurasia to the Arctic. Ambio 20, 293–297.
Park, J.-S., Shin, S.-K., Kim, W.-I., Kim, B.-H., 2011. Residual levels and identify possible sources of organochlorine pesticides in Korea atmosphere. Atmos. Environ. 45, 7496–7502.
Qiao, L.-N., Zhang, Z.-F., Liu, L.-Y., Song, W.-W., Ma, W.-L., Zhu, N.-Z., Li, Y.-F., 2019. Measurement and modeling the gas/particle partitioning of organochlorine pesticides (OCPs) in atmosphere at low temperatures. Sci. Total Environ. 667, 318–324.
Qiu, X., Zhu, T., Yao, B., Hu, J., Hu, S., 2005. Contribution of dicofol to the current DDT pollution in China. Environ. Sci. Technol. 39, 4385–4390.
Qu, C., Xing, X., Albanese, S., Doherty, A., Huang, H., Lima, A., Qi, S., De Vivo, B., 2015. Spatial and seasonal variations of atmospheric organochlorine pesticides along the plain-mountain transect in central China: regional source vs. long-range transport and air–soil exchange. Atmos. Environ. 122, 31–40.
Shen, L., Wania, F., 2005. Compilation, evaluation, and selection of physical−chemical property data for organochlorine pesticides. J. Chem. Eng. Data 50, 742–768.
Shen, L., Wania, F., Lei, Y.D., Teixeira, C., Muir, D.C.G., Bidleman, T.F., 2005. Atmospheric distribution and long-range transport behavior of organochlorine pesticides in North America. Environ. Sci. Technol. 39, 409–420.
Shoeib, M., Harner, T., 2009. Using measured octanol-air partition coefficients to explain environmental partitioning of organochlorine pesticides. Environ. Toxicol. Chem. 21, 984–990.
Shunthirasingham, C., Oyiliagu, C.E., Cao, X., Gouin, T., Wania, F., Lee, S.-C., Pozo, K., Harner, T., Muir, D.C.G., 2010. Spatial and temporal pattern of pesticides in the global atmosphere. J. Environ. Monit. 12, 1650–1657.
Sofuoglu, A., Cetin, E., Bozacioglu, S.S., Sener, G.D., Odabasi, M., 2004. Short-term variation in ambient concentrations and gas/particle partitioning of organochlorine pesticides in Izmir, Turkey. Atmos. Environ. 38, 4483–4493.
Stojić, A., Stanišić Stojić, S., 2017. The innovative concept of three-dimensional hybrid receptor modeling. Atmos. Environ. 164, 216–223.
Sun, P., Blanchard, P., Brice, K., Hites, R.A., 2006. Atmospheric organochlorine pesticide concentrations near the Great Lakes: temporal and spatial trends. Environ. Sci. Technol. 40, 6587–6593.
Syed, J.H., Malik, R.N., Liu, D., Xu, Y., Wang, Y., Li, J., Zhang, G., Jones, K.C., 2013. Organochlorine pesticides in air and soil and estimated air-soil exchange in Punjab, Pakistan. Sci. Total Environ. 444, 491–497.
Takazawa, Y., Takasuga, T., Doi, K., Saito, M., Shibata, Y., 2016. Recent decline of DDTs among several organochlorine pesticides in background air in East Asia. Environ. Pollut. 217, 134–142.
Tian, C., Ma, J., Liu, L., Jia, H., Xu, D., Li, Y.-F., 2009. A modeling assessment of association between East Asian summer monsoon and fate/outflow of α-HCH in Northeast Asia. Atmos. Environ. 43, 3891–3901.
Tian, L., Li, J., Zhao, S., Tang, J., Li, J., Guo, H., Liu, X., Zhong, G., Xu, Y., Lin, T., Lyv, X., Chen, D., Li, K., Shen, J., Zhang, G., 2021. DDT, chlordane, and hexachlorobenzene in the air of the Pearl River Delta revisited: a tale of source, history, and monsoon. Environ. Sci. Technol. 55, 9740–9749.
Van de Plassche, E., Schwegler, A., Rasenberg, M., Schoulten, G., 2001. PentaChlorobenzene. Nomination Dossier for Inclusion in the Stockholm Convention on Persistent Organic Pollutants (POPs). United Nations Environment Program (UNEP), Switzerland.
Walker, K., Vallero, D.A., Lewis, R.G., 1999. Factors influencing the distribution of lindane and other hexachlorocyclohexanes in the environment. Environ. Sci. Technol. 33, 4373–4378.
Wang, B., Iino, F., Yu, G., Huang, J., Wei, Y., Yamazaki, N., Chen, J., Chen, X., Jiang, W., Morita, M., 2010a. HRGC/HRMS analysis of mirex in soil of Liyang and preliminary assessment of mirex pollution in China. Chemosphere 79, 299–304.
Wang, C., Wang, X., Gong, P., Yao, T., 2018a. Long-term trends of atmospheric organochlorine pollutants and polycyclic aromatic hydrocarbons over the southeastern Tibetan Plateau. Sci. Total Environ. 624, 241–249.
Wang, G., Lu, Y., Han, J., Luo, W., Shi, Y., Wang, T., Sun, Y., 2010b. Hexachlorobenzene sources, levels and human exposure in the environment of China. Environ. Int. 36, 122–130.
Wang, L., Cao, G., Liu, L.-Y., Zhang, Z.-F., Jia, S.-M., Fu, M.-Q., Ma, W.-L., 2023. Cross-regional scale studies of organochlorine pesticides in air in China: pollution characteristic, seasonal variation, and gas/particle partitioning. Sci. Total Environ. 904, 166709.
Wang, P., Meng, W., Li, Y., Zhang, Q., Zhang, L., Fu, J., Yang, R., Jiang, G., 2018b. Temporal variation (2011–2014) of atmospheric OCPs at King George Island, West Antarctica. Atmos. Environ. 191, 432–439.
Wang, X.P., Sheng, J.J., Gong, P., Xue, Y.G., Yao, T.D., Jones, K.C., 2012. Persistent organic pollutants in the Tibetan surface soil: spatial distribution, air-soil exchange and implications for global cycling. Environ. Pollut. 170, 145–151.
Wania, F., Haugen, J.-E., Lei, Y.D., Mackay, D., 1998. Temperature dependence of atmospheric concentrations of semivolatile organic compounds. Environ. Sci. Technol. 32, 1013–1021.
Wania, F., Mackay, D., 1993. Global fractionation and cold condensation of low volatility organochlorine compounds in polar regions. Ambio 22, 10–18.
Willett, K.L., Ulrich, E.M., Hites, R.A., 1998. Differential toxicity and environmental fates of hexachlorocyclohexane isomers. Environ. Sci. Technol. 32, 2197–2207.
Ya, M., Wu, Y., Wu, S., Li, Y., Mu, J., Fang, C., Yan, J., Zhao, Y., Qian, R., Lin, X., Wang, X., 2019. Impacts of seasonal variation on organochlorine pesticides in the East China Sea and Northern South China Sea. Environ. Sci. Technol. 53, 13088–13097.
Yang, Y., Li, D., Mu, D., 2008. Levels, seasonal variations and sources of organochlorine pesticides in ambient air of Guangzhou, China. Atmos. Environ. 42, 677–687.
Yeo, H.-G., Choi, M., Sunwoo, Y., 2004. Seasonal variations in atmospheric concentrations of organochlorine pesticides in urban and rural areas of Korea. Atmos. Environ. 38, 4779–4788.

Yu, H., Liu, Y., Shu, X., Ma, L., Pan, Y., 2020. Assessment of the spatial distribution of organochlorine pesticides (OCPs) and polychlorinated biphenyls (PCBs) in urban soil of China. Chemosphere 243, 125392.
Yu, S.Y., Liu, W.J., Xu, Y.S., Zhao, Y.Z., Cai, C.Y., Liu, Y., Wang, X., Xiong, G.N., Tao, S., Liu, W.X., 2019. Organochlorine pesticides in ambient air from the littoral cities of northern China: spatial distribution, seasonal variation, source apportionment and cancer risk assessment. Sci. Total Environ. 652, 163–176.
Zhan, L., Lin, T., Wang, Z., Cheng, Z., Zhang, G., Lyu, X., Cheng, H., 2017. Occurrence and air-soil exchange of organochlorine pesticides and polychlorinated biphenyls at a CAWNET background site in central China: implications for influencing factors and fate. Chemosphere 186, 475–487.
Zhang, L., Dong, L., Yang, W., Zhou, L., Shi, S., Zhang, X., Niu, S., Li, L., Wu, Z., Huang, Y., 2013. Passive air sampling of organochlorine pesticides and polychlorinated biphenyls in the Yangtze River Delta, China: concentrations, distributions, and cancer risk assessment. Environ. Pollut. 181, 159–166.
Zhang, N., Yang, Y., Liu, Y., Tao, S., 2009. Determination of octanol-air partition coefficients and supercooled liquid vapor pressures of organochlorine pesticides. J. Environ. Sci. Health B 44, 649–656.